Microsc. Microanal. 23, 1096–1106, 2017
doi:10.1017/S1431927617012697

Microscopy AND Microanalysis

© MICROSCOPY SOCIETY OF AMERICA 2017

Depth Resolution Dependence on Sample Thickness and Incident Energy in On-Axis Transmission Kikuchi Diffraction in Scanning Electron Microscope (SEM)

Etienne Brodu,[1,2] and Emmanuel Bouzy[1,2,*]

[1] *Laboratoire d'Etude des Microstructures et de Mécanique des Matériaux (LEM3), UMR CNRS 7239, Université de Lorraine, 57045 Metz, France*
[2] *Laboratory of Excellence on Design of Alloy Metals for low-MAss Structures (DAMAS), University of Lorraine, 57045 Metz, France*

Abstract: Transmission Kikuchi diffraction is an emerging technique aimed at producing orientation maps of the structure of materials with a nanometric lateral resolution. This study investigates experimentally the depth resolution of the on-axis configuration, via a twinned silicon bi-crystal sample specifically designed and fabricated. The measured depth resolution varies from 30 to 65 nm in the range 10–30 keV, with a close to linear dependence with incident energy and no dependence with the total sample thickness. The depth resolution is explained in terms of two mechanisms acting concomitantly: generation of Kikuchi diffraction all along the thickness of the sample, associated with continuous absorption on the way out. A model based on the electron mean free path is used to account for the dependence with incident energy of the depth resolution. In addition, based on the results in silicon, the use of the mean absorption coefficient is proposed to predict the depth resolution for any atomic number and incident energy.

Key words: Depth resolution, mean absorption coefficient, transmission Kikuchi diffraction (TKD), electron diffraction, scanning electron microscope (SEM)

Introduction

Transmission Kikuchi diffraction (TKD) in scanning electron microscope (SEM) is a recent technique derived from electron backscatter diffraction (EBSD) (Keller & Geiss, 2012; Sneddon et al., 2016). With the TKD technique, Kikuchi diffraction is produced in transmission with electron-transparent samples and patterns are typically recorded with a phosphor screen mounted on a charged-coupled device (CCD) or complementary metal-oxide-semiconductor camera (a promising emerging alternative is by direct detection (Wilkinson et al., 2013; Vespucci et al., 2015, 2017)). The patterns are then indexed to produce orientation maps, from which exhaustive microstructural information is available.

The improvement in lateral resolution compared to EBSD enables the possibility of studying much finer microstructures, the lateral resolution of the TKD technique being below 10 nm (Keller & Geiss, 2012; Trimby, 2012; Brodusch et al., 2013; Brodu et al., 2017). The lateral resolution of the TKD technique is typically investigated either via Monte Carlo simulation, which can accurately determine the lateral spread of the electrons scattered in a material (van Bremen et al., 2016; Wang et al., 2016), or experimentally via the determination of the lateral distance separating two unconvoluted diffraction patterns (Trimby, 2012; Fundenberger et al., 2016; Brodu et al., 2017). From these studies, it was easily seen that the lateral resolution is at its best at high incident energy and low sample thickness.

However, if one wants to determine the source volume of material with which to associate the information contained in a diffraction pattern, knowing the lateral resolution is not enough, one has to determine the depth resolution as well. For this reason, the determination of the depth resolution has attracted a large interest, and was investigated in the frame of EBSD in SEM (Ren et al., 1998; Dingley, 2004; Zaefferer, 2007; Deal et al., 2008; Bhattacharyya & Eades, 2009; Wisniewski et al., 2017), for electron channeling pattern in SEM (Yamamoto, 1977) and since recently for TKD in SEM (Suzuki, 2013; Rice et al., 2014; Trimby et al., 2014).

The depth resolution of EBSD was investigated experimentally via the use of thin amorphous layers deposited on bulk materials (Zaefferer, 2007; Wisniewski et al., 2017). Alternatively, some authors propose to evaluate the depth resolution from the angular width of the Kikuchi lines (Dingley, 2004; Zaefferer, 2007). A few values of depth resolution are available. They range from about 10 nm (Dingley, 2004; Zaefferer, 2007) to several tens of nanometers (Wisniewski et al., 2017). Then, Deal et al. (2008) showed via filtering experiments, following a suggestion by Ren et al. (1998), that the electrons contributing the most to the Kikuchi patterns are low-loss electrons. From this result, it was deduced that the source volume for Kikuchi diffraction is smaller than the whole interaction volume. Finally, two main options are investigated to improve the depth resolution of EBSD: (1) energy filters can improve the depth resolution by selecting low-loss electrons with short path lengths and thus low penetration depths (Deal et al., 2008;

Received July 28, 2017; accepted October 27, 2017
*Corresponding author. emmanuel.bouzy@univ-lorraine.fr

https://doi.org/10.1017/S1431927617012697 Published online by Cambridge University Press

Bhattacharyya & Eades, 2009) and (2) the use of a low incident energy also reduces the penetration depth and improves the depth resolution (Ren et al., 1998).

If the existence of a depth resolution, or selectivity, was obvious for EBSD because electrons penetrate a bulk material only for a given depth anyway, the depth resolution in transmission with TKD was less obvious because electron–matter interactions occur across the whole thickness. Suzuki (2013) produced a first solid proof: an orientation map produced by TKD on a lamella matching the EBSD map obtained from the back face of the same lamella. More evidence of selectivity can be found in Trimby et al. (2014), where it is highlighted that many grains displayed in orientation maps are much smaller than the thickness of the lamella. Then, Rice et al. (2014) showed with amorphous layers that the scattering of prime importance for the formation of Kikuchi patterns occurs near the back surface. Although the depth resolution of the TKD technique was observed, it has not yet been quantified, and the mechanisms involved are not clearly identified. Therefore, this study intends to quantify the depth resolution of the on-axis configuration of the TKD technique for the first time on cubic silicon, determine its dependence with incident energy and sample thickness, and propose a physical model. Because the depth resolution probably depends on the beam-sample-detector geometry, the depth resolution of the classical TKD configuration (i.e., with a detector vertical like for EBSD) might be different (and better), as outlined by Trimby et al. (2014).

Experimental

On-Axis TKD Set-Up

This study was performed with a field emission gun SEM Zeiss Supra 40 (Zeiss, Oberkochen, Germany) equipped with an on-axis TKD system that consists of a Bruker e-Flash^{1000} (Bruker) camera mounted on a Bruker OPTIMUS^{TM} (Bruker, Billerica, MA, USA) detector head. The specificity of this detector head is that the scintillator is set horizontally instead of vertically like in the conventional TKD system (Fig. 1). This on-axis detector was first designed, built and tested at LEM3 (Fundenberger et al., 2016) and is now commercialized by Bruker under the name OPTIMUS^{TM}. With this on-axis configuration, the sample is set perpendicular to the electron beam, with the horizontal scintillator set underneath it in order to collect the electrons transmitted through the sample. The on-axis TKD in SEM is thus similar to the orientation mapping from Kikuchi diffraction developed for TEM (Fundenberger et al., 2003; Morawiec et al., 2014). The diffraction patterns formed on the scintillator are then captured by the CCD camera, which remains vertical in the camera block, via a mirror inclined at 45°. The main advantage of this configuration is that the scintillator is positioned in the direction of maximum signal intensity, enabling a very high acquisition speed (Yuan et al., 2017), while the lateral resolution is expected to be at least as good as conventional TKD (Brodu et al., 2017). With on-axis TKD, the distance between the detector and the sample is adjustable, typically in the range 5–30 mm, which allows adjustment of the range of solid angle observed in reciprocal space. This distance is adjusted by tilting the full camera block. The consequence is that the scintillator does not remain exactly perpendicular to the electron beam, although it remains in the range 90° ± 2° degrees for a detector-sample distance in the range 5–30 mm. The acquisition parameters are listed in the caption for each figure showing diffraction patterns.

Sample Design and Preparation

A focused ion beam (FIB) lamella was specifically designed and fabricated for the determination of the depth resolution in on-axis TKD. This lamella is composed of two twinned cubic silicon crystals, whose twin boundary makes a low angle relative to the surface. The point with such a lamella is that the in-depth position of the twin boundary inside the lamella is known for all locations, because the twin boundary is a straight plane. For the preparation of the lamella, a Si wafer presenting multiple twins was selected. Then, an area of the wafer containing a roughly perpendicular twin boundary relative to the surface was identified. The perpendicularity was simply evaluated from the twin boundary

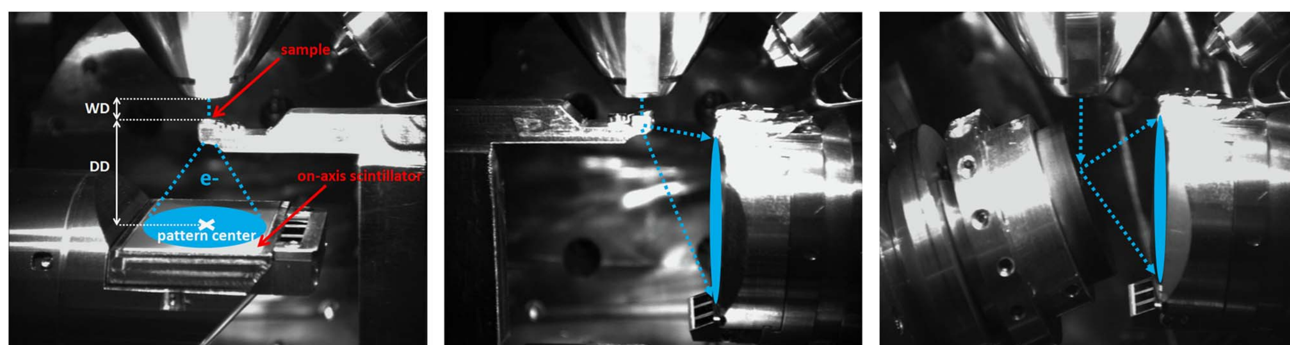

Figure 1. On-axis transmission Kikuchi diffraction (TKD) configuration (left) and comparison with conventional TKD (middle) and electron backscatter diffraction (EBSD) (right) in scanning electron microscope (SEM). Note that the chamber holds two EBSD cameras simultaneously, each on its own port, one for EBSD and conventional TKD, the other one being dedicated to on-axis TKD.

https://doi.org/10.1017/S1431927617012697 Published online by Cambridge University Press

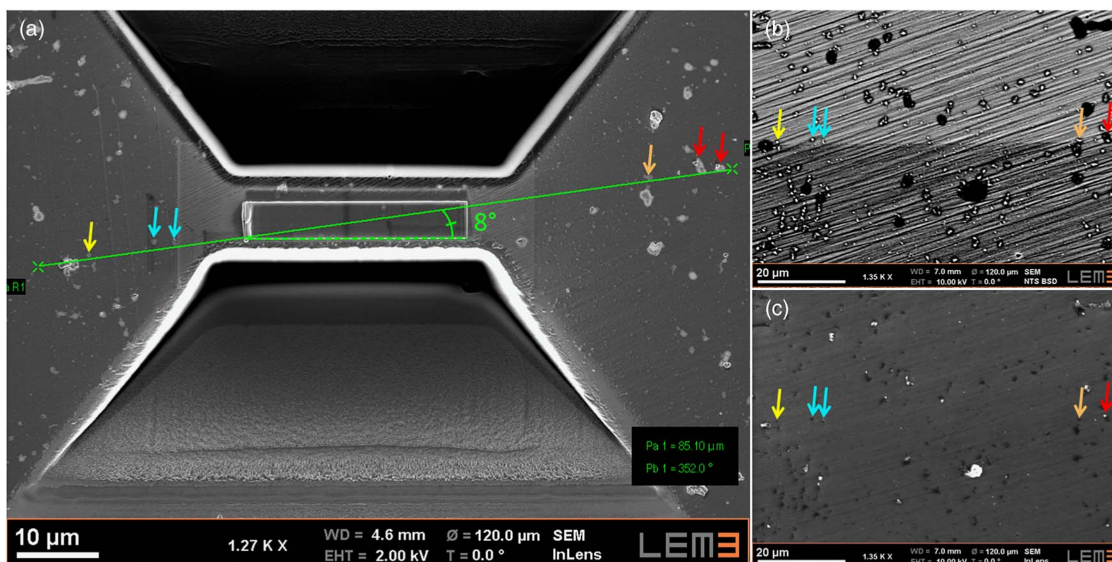

Figure 2. **a:** Side view of the Si lamella being excavated by focused ion beam. The solid green line indicates the positioning of the twin boundary, which is tilted by 8° relative to the surface of the lamella. **b**: Direct view of the twin boundary with backscattered electrons (BSD detector) in the same area, before excavation. The arrows indicate details on the surface that were used to track the position of the twin boundary. **c:** Same view as (**b**) but with secondary electrons (InLens detector); the boundary is no more visible, hence the need for details on the surface used as landmarks.

leaving two traces (one on each side of the wafer) that looked vertically aligned. Inside this selected area, a FIB lamella was then extracted in a way to induce a low angle between the twin boundary and the surface of the lamella. This angle could simply be controlled by rotating the milling frame relative to the boundary on the surface of the wafer in the FIB, as seen in Figure 2. In the meantime, the twin boundary is assumed to be roughly perpendicular to the observation plane in Figure 2 (bear in mind that Fig. 2 presents a side view of the lamella being excavated). During the excavation, the angle of the twin boundary with the surface of the lamella was thus perfectly known, and was purposely set to 8°. The next steps consisted in the typical lift-out, transfer to a grid and thinning of the lamella. During these final preparation steps, the exact positioning of the twin boundary in the lamella was lost, especially during the thinning step. However, the angle of the twin boundary with the surface of the lamella remained largely unchanged. Besides, as it is detailed in the Methodology for the Determination of the Depth Resolution section, the position of the twin boundary could be determined by diffraction later on. The last step consisted in applying a low energy cleaning at 5 keV, 240 pA for 60 s on each side in order to remove as much as possible the amorphous layer induced by the milling at 30 keV. With such final polishing, we estimate that there is about 5 nm of amorphous Si on each side of the lamella according to Tee (Tee et al., 2009). Because this layer is likely thin, but also because we have no way to measure its thickness, it is neglected for the remainder of the study. (Note that the thicker the amorphous layer, the more underestimated, i.e. shorter, the depth resolution would be with the present methodology.) At this point, the thickness of the lamella was largely unknown, but seemed to range from under 100 nm up to

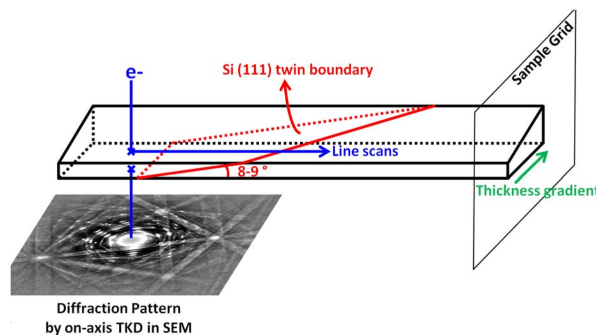

Figure 3. Scheme of the Si lamella produced by FIB and used for the determination of the depth resolution in on-axis transmission Kikuchi diffraction (TKD). SEM, scanning electron microscope.

220 nm according to side views, with a thickness gradient across the lamella (Fig. 3). This thickness variation, although first unintended, was then purposely not corrected by additional milling. This way, it became possible to study the dependence of the depth resolution with the sample thickness. For this, the local thickness of the lamella at the point of measurement of the depth resolution is determined according to the methodology described in the next section.

Methodology for the Determination of the Depth Resolution

Every time the text refers to the depth resolution, we are using the following definition: we define the depth resolution in TKD as the minimal thickness of material at the bottom of the sample such that the material above does not produce a contribution to the Kikuchi diffraction pattern that can be detected, in the general case by analysis software, but in the

https://doi.org/10.1017/S1431927617012697 Published online by Cambridge University Press

present study by the naked eye. By this definition, the depth resolution is also the minimal thickness of material at the bottom of the sample contributing alone to the Kikuchi diffraction pattern. This definition presents the depth resolution as a finite length, although it results from a continuous absorption process as discussed in the next sections. The depth resolution only becomes a finite length when the limitations of the hardware and software are introduced. Thus, it can be expected that the depth resolution determined experimentally will depend on the hardware used (S/N ratio, sensitivity, dynamic range), the acquisition parameters (integration time and image averaging in particular, and maybe even pattern resolution), and the software (ability to extract the signal from the noise with the dynamic background correction and detection threshold). The consequence is that a depth resolution value is not an intrinsic property. With this limitation in mind, this study mostly intends to produce depth resolution values that are relevant to the production of orientation maps with current technology (see On-Axis TKD Set-Up section for details on the experimental set-up). Most importantly, the results will allow us to draw general conclusions in terms of dependence with sample thickness and incident energy, i.e. independent on hardware, software, and acquisition parameters.

With the twinned cubic Si bi-crystal, the depth resolution, according to the definition above, was determined experimentally in a straightforward way, with limited hypotheses. The process consisted of recording diffraction patterns in the area of the twin boundary and then analyzing patterns along a straight line crossing the twin (see Figs. 3, 4). The key principle is that, while the twin boundary moves closer to the top surface (i.e., the surface of incidence of the beam) and further from the bottom surface, the depth resolution becomes equal to the distance between the twin boundary and the back surface at the point where the pattern stops containing Kikuchi diffraction information associated to the top crystal. In order to determine the depth resolution, it only requires at that point to determine the corresponding in-depth position of the twin boundary. This determination can be done because a twin boundary forms a straight plane, and is thus predictable; all we need to know is the position of the intersection of the twin boundary with the back surface and the angle that the twin boundary forms with the surface. The angle that the twin boundary forms with the surface was determined in two ways: (1) in the beginning steps of the FIB preparation of the lamella, the angle is chosen (hence known, see Fig. 2). During the following steps of FIB preparation, until the final thinning and low-keV cleaning, special care was taken to ensure that this angle was maintained. (2) Alternatively, this angle was also calculated from the orientation of the two twinned crystals in the final lamella. Typical diffraction patterns of each crystal were recorded by on-axis TKD and indexed. Once their orientation was known, the angle could be determined because we know that the twin boundary is a (111) plane. With this second method, the angle was found to be 9.2°. A difference of 1° between the two values is reasonable and can very well be explained by the geometric tolerances of the systems. An intermediate value of 8.5° was selected and kept constant for all calculations in the remainder of the study. The second unknown is the position of the intersection of the twin boundary with the back surface. This determination was done by analysis of the diffraction patterns. We determined this intersection as the point where the very first emerging diffraction spots associated to the bottom crystal were observed in diffraction patterns (point 2 in Fig. 4). We base this determination on the fact that very little material is required to produce diffraction spots (Germer, 1939) and propose that it should produce a very limited error.

The thickness of the lamella at the exact location of measurement of the depth resolution is also useful to know. This way, the dependence of the depth resolution with sample thickness can be studied. The determination of the total lamella thickness could be performed, but unlike for the determination of the depth resolution, the position of the intersection of the twin boundary with the top surface needs to be known. We also assumed that the very first appearance of diffraction spots, here associated to the top crystal, marked the position of this intersection (point 8 in Fig. 4).

Finally, a difficult methodology question concerned the evaluation of the disappearing of the Kikuchi diffraction associated to the top crystal. Quantitative analysis of the fading of the band contrast with a software was unsuccessful, both with the patterns and the Hough transform, because of the difficulty to isolate information (i.e., the bands specifically associated to the top crystal), in particular when the contrast becomes low. The fading of a given Kikuchi band tends to blend with other intensity variations, like the one of nearby spots and more importantly with the generation of new nearby bands associated to the bottom crystal. Hence, it was done with the naked eye. What is gained here in terms of critical analysis of the patterns and ability to isolate information, is lost in terms of quantified threshold and reproducibility.

Results and Discussion

Diffraction Pattern Evolution Along a Straight Line Crossing the Twin Boundary

Before we present the actual values of the depth resolution by on-axis TKD on cubic silicon and the dependence with incident energy and sample thickness, this subsection presents the evolution of the diffraction pattern along a straight line scan crossing the twin boundary. This line scan is such that the in-depth position of the twin boundary under the incident beam varies with the lateral position of the beam on the surface, as displayed in Figure 4. The full sequence of diffraction patterns is presented, for an incident energy of 30 keV. Some features discussed below might not be well visible in the patterns displayed in Figure 4. However, even the tiniest and most subtle changes become very well visible to the naked eye when the patterns are scrolled inside a fixed

https://doi.org/10.1017/S1431927617012697 Published online by Cambridge University Press

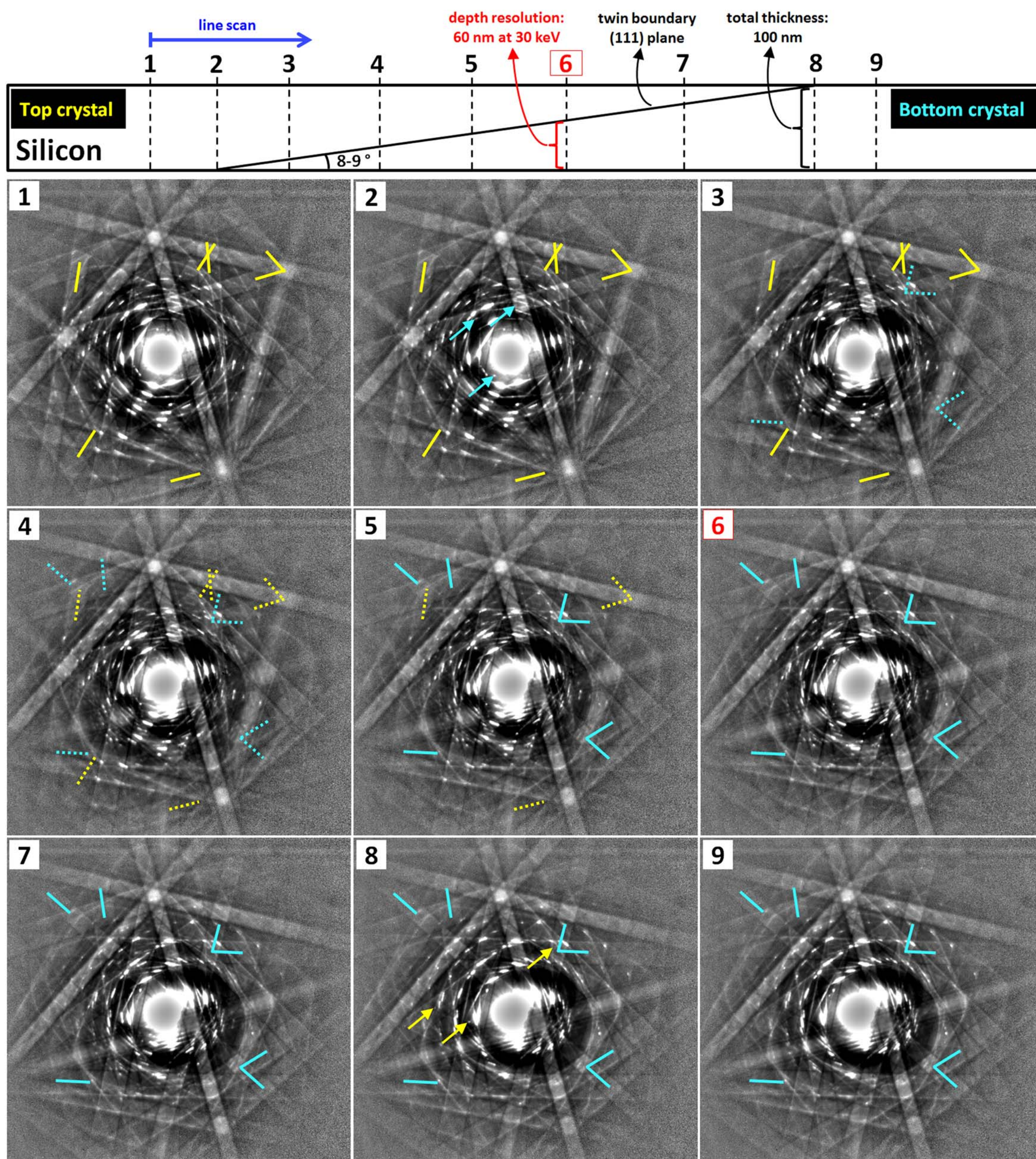

Figure 4. Evolution of the diffraction pattern along a particular line scan crossing a cubic silicon twin boundary in on-axis transmission Kikuchi diffraction in scanning electron microscope at 30 keV. Thanks to the twin boundary plane being inclined by a few degrees relative to the surface of the FIB lamella, the in-depth position of the twin boundary under the incident beam varies (and is known) along the line scan. The arrows in patterns 2 and 8 mark the very first appearance of spots associated to the other crystal. The solid lines in the patterns indicate bands of interest, along their length, associated specifically to the top or bottom crystal depending on the color (bands shared by both crystals are disregarded). When bands are close to disappearing from the patterns, they are indicated with dotted lines instead. Acquisition parameters: incident energy: 30 keV; objective aperture: 90 μm—low current mode (about 2.4 nA); sample thickness for this specific line scan: 100 nm; pattern resolution: 600 × 600 pixels; integration time: 18 ms; image averaging: 12 × (216 ms total per pattern); distance detector-sample: 27.5 mm. The pattern background correction is performed by ESPRIT 2.0 by Bruker.

frame, in particular the very first emergence of new diffraction spots. Both the high quality of patterns, thanks to appropriate acquisition parameters, and the stability of patterns, thanks to very few crystal defects, also helped tremendously to identify subtle variations in patterns induced by the in-depth motion of the twin boundary.

We assumed for the determination of the depth resolution that the two intersections of the twin boundary with the top and bottom surfaces were met as soon as the very first spots associated to the other crystal were detected in diffraction patterns (see Methodology for the Determination of the Depth Resolution section). This is typically the case in

https://doi.org/10.1017/S1431927617012697 Published online by Cambridge University Press

the patterns 2 and 8 in Figure 4. Very shortly after point 2, while the diffraction spots are still progressively developing with the increase in thickness of the bottom crystal, a faint Kikuchi band contrast associated to the bottom crystal appears as well. The thickness interval inside which the diffraction from the bottom crystal consists only of spots is not measurable because it is too narrow (i.e., the Kikuchi diffraction very closely follows the spots). The Kikuchi diffraction associated to the bottom crystal then builds very progressively as the thickness of the bottom crystal increases. In the meantime, while the twin boundary gets further away from the bottom surface, the Kikuchi diffraction associated to the top crystal progressively decreases in contrast and fades. There is thus, a bottom crystal thickness for which the Kikuchi diffractions associated to the two crystals are somehow equivalent in contrast. This point of balance seems to be reached somewhere around the point 4 in Figure 4 and seems to correspond roughly to half of the depth resolution. This thickness, for which the two Kikuchi diffractions of these two crystals are equivalent in contrast, will typically be the one for which the indexing will swing from one orientation to the other in orientation maps (note that the progressive generation of the Kikuchi diffraction associated to the bottom crystal and the fading of the Kikuchi diffraction of the top crystal are most likely the product of two very separate physical mechanisms, which means there is no reason for this point of balance to necessarily be halfway). With further increasing thickness of the bottom crystal, there is finally a point where the Kikuchi diffraction associated to the top crystal is no longer visible in patterns. It corresponds to point 6. Here, we consider that the depth resolution is equal to the thickness of the bottom crystal. At point 6, there remains enough top crystal to produce Kikuchi diffraction (about 40 nm for the particular line scan in Figure 4, but even more for many other line scans, see Fig. 5), and still, no information in the forms of a Kikuchi diffraction associated to the top crystal is visible in patterns. Only the spots associated to the top crystal remain visible, until point 8, which is much further in terms of lateral positioning of the beam. The depth resolution of the Kikuchi diffraction in TKD is here evidenced without ambiguity, and as expected, TKD does not *see* the crystal that is above the depth resolution.

While this aspect of the depth resolution is made clear, a new question emerges and remains open: what does TKD see *inside* that depth resolution layer? The description above of the evolution of the diffraction pattern along a line scan showed that two mechanisms are active inside the depth resolution layer: fading but also generation of Kikuchi diffraction. While the fading is here well studied and its dependence with energy identified (see Towards a Physical Model for the Depth Resolution section), the progressive generation with increasing crystal thickness could not be determined with the same accuracy and its dependence with incident energy remains unknown as of now. Consequently, we do not know how these two characteristic lengths interact. While it seems that the generation of Kikuchi diffraction occurs over a thickness shorter than is needed for absorption, maybe

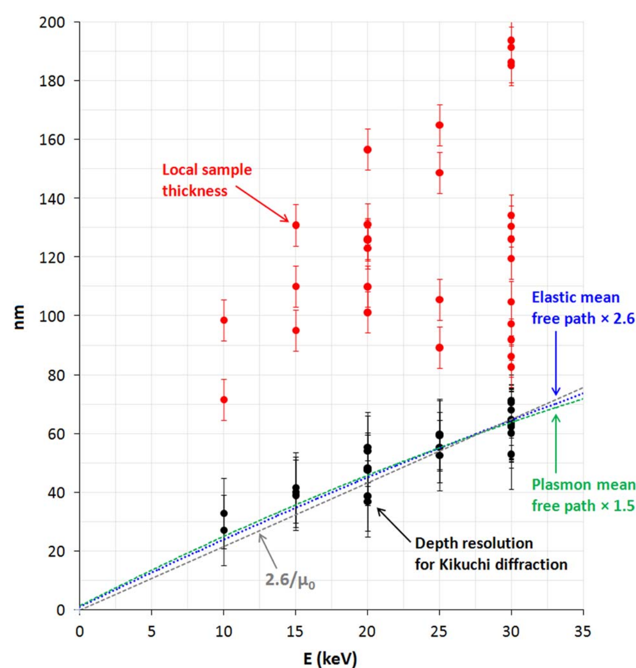

Figure 5. Depth resolution dependence with sample thickness and incident energy by on-axis transmission Kikuchi diffraction (TKD) in scanning electron microscope for cubic Si. For each incident energy, the depth resolution was measured at different locations on the Si lamella, with the objective to vary the local sample thickness. The red dots are the local sample thickness at the point of measurement of the depth resolution. The depth resolution in on-axis TKD appears to have a close to linear dependence with incident energy, but no dependence with sample thickness. The elastic and plasmon mean free paths are taken from Mayol & Salvat (1997) and Shinotsuka et al. (2015), respectively, and the mean absorption coefficient is obtained from Reimer (1997: 309).

there could be a scenario (i.e., atomic number and energy) for which it would be the opposite. Maybe in that case only blurred, partially generated patterns could be produced, even by a perfect single crystal. As of now, before further studies, a very approximate answer to the question "what does TKD see *inside* that depth resolution layer" is: a portio of all crystals/grains in variable proportions depending on their size, because it determines the generation part, and their in-depth position inside the depth resolution layer, because it determines the fading part. In particular, a crystal/grain right at the back surface will not always necessarily be the one contributing the most to the Kikuchi pattern. For example, a small grain right at the back surface can contribute less than a bigger grain further away from the back surface. It was precisely the case between point 2 and 4 in Figure 4, where the most visible crystal was actually the top crystal even though the bottom crystal is present right at the back surface.

Depth Resolution Dependence With Sample Thickness and Incident Energy

The depth resolution in on-axis TKD as a function of sample thickness and incident energy determined using the

https://doi.org/10.1017/S1431927617012697 Published online by Cambridge University Press

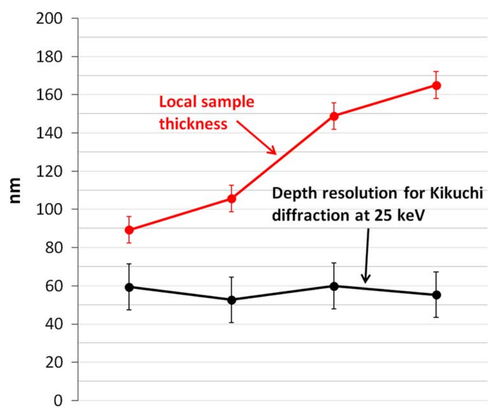

Figure 6. Depth resolution dependence with sample thickness at 25 keV by on-axis transmission Kikuchi diffraction in scanning electron microscope for cubic Si. The values are the same as in Figure 5, only displayed differently.

methodology presented in Methodology for the Determination of the Depth Resolution section is presented in Figure 5 for cubic silicon. The dependence with sample thickness could be studied thanks to the thickness gradient produced during the FIB thinning of the Si lamella (Fig. 3). In the low incident energy range, large thicknesses could not be tested because of the disappearing of diffraction spots from patterns, spots on which we rely for the determination of the depth resolution and sample thickness (see Methodology for the Determination of the Depth Resolution section). For example, at 10 keV on Si, a thickness of about 100 nm is the upper limit that could be tested, in agreement with a previous study on the thickness and energy dependence of the absorption of diffraction spots (Brodu et al., 2017). A larger range of thickness could be tested at 30 keV. The uncertainty displayed in Figure 5 for the depth resolution almost fully results from the difficulty to determine when the Kikuchi diffraction associated to the top crystal is no more present in patterns. Similarly, the uncertainty for the local sample thickness results from the determination of the first emergence of spots. According to the results presented in Figures 5 and 6, the depth resolution seems largely independent from the sample thickness in the range 70–200 nm. The absence of dependence with sample thickness of the depth resolution is good news because the sample thickness is often unknown in everyday TKD experiments. On the other hand, the depth resolution presents a clear dependence with incident energy in the range 10–30 keV, with a close to linear dependence, as discussed in the next section. This dependence opens the door to the tuning of the depth resolution via the choice of incident energy, although it might be difficult to take advantage of this dependence because of the simultaneous, and opposite effect on the lateral resolution.

Towards a Physical Model for the Depth Resolution

Diffraction Pattern Evolution Along a Straight Line Crossing the Twin Boundary section showed that the Kikuchi diffraction produced by a crystal disappears progressively from diffraction patterns when another crystal of increasing thickness is added underneath it. In particular, when the bottom crystal thickness reaches the depth resolution, the Kikuchi diffraction produced by the top crystal is no more visible in patterns. We can expect this behavior to result from the subsequent interaction of the Kikuchi diffraction produced by the top crystal along the travel inside the bottom crystal. These interactions are of two main types: (1) incoherent interaction with plasmon and phonon (other electron–electron interactions can be neglected) and (2) elastic interaction. In the case of Bragg diffraction, the contribution of the elastic interaction to the depletion of the wave produced by the top crystal along the travel inside the bottom crystal is clearly visible in Figure 7, with the presence of spots resulting from double diffraction. All three electron–matter interactions involved here (elastic, plasmon, phonon) have in common a close to linear dependence with energy of their mean free paths (Hall & Hirsch, 1965; Crewe et al., 1970; Williams & Barry Carter, 1996; Mayol & Salvat, 1997; Tanuma et al., 2011; Shinotsuka et al., 2015). According to this dependence of the mean free paths, if we imagine that a specific number of interactions is necessary to make the Kikuchi diffraction associated to the top crystal disappear from patterns, then it could be expected that the depth resolution measured would also show a close to linear dependence with energy. In addition, in this scenario, the depth resolution should be independent of the total sample thickness. This latter prediction was confirmed in Depth Resolution Dependence With Sample Thickness and Incident Energy section. As for the former prediction, Figure 5 shows that the mean free path for plasmon (Shinotsuka et al., 2015) and elastic scattering (Mayol & Salvat, 1997), as a function of incident energy multiplied by a constant number, fits the experimental results of depth resolution. Yamamoto (1977) also identified a linear dependence of the depth resolution in electron channeling patterns in the SEM on Al and Cr. The meaning of the multiplication constant is here straightforward: this constant consists in the average number of collisions per electron occurring along the travel path corresponding to the depth resolution; 1.5 plasmon and 2.6 elastic interactions here for cubic Si. Values of the mean free path for phonon scattering could not be found for Si in the right energy range, hence, it is not plotted. Since the energy dependence of all three interactions have similar dependencies with incident energy, it is not possible to discriminate between the respective responsibilities of these interactions from this study (i.e., to attribute the depth resolution to one interaction over another). At low energy ($\leq$15 keV), the values seem to drift apart from the model, but this might very well be explained by the beam broadening. Indeed, it is expected that the beam broadening at low energy would lead to an overestimation of the depth resolution, as illustrated in Figure 8 via Monte Carlo simulations [CASINO (Drouin et al., 2007)]. Although Figure 8 is mostly intended for illustration, it is accurate in terms of geometry and electron trajectory. From it, one can tell that the beam broadening could very well induce a bias in the determination of the

https://doi.org/10.1017/S1431927617012697 Published online by Cambridge University Press

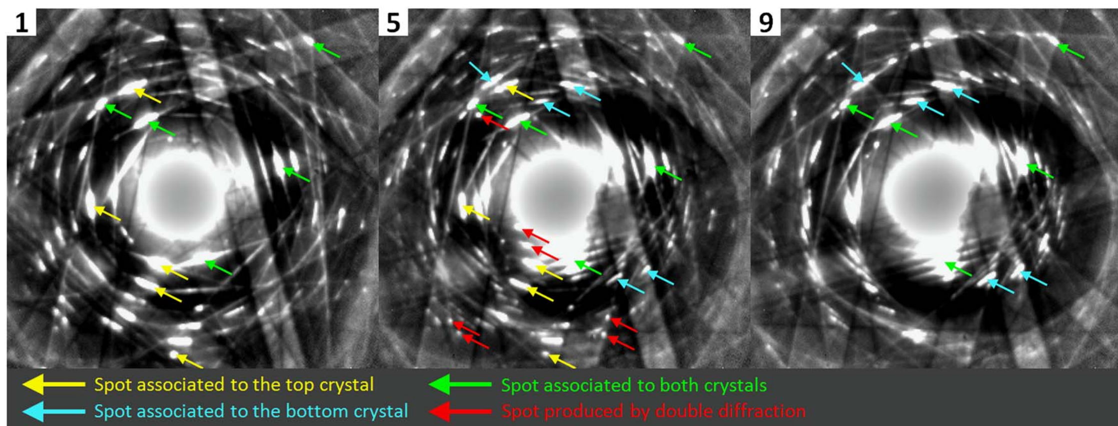

Figure 7. Zoom in the patterns 1, 5, and 9 from Figure 4. Many spots produced by double diffraction are visible in the pattern 5. These spots are the product of the diffraction, in the bottom crystal, of the diffracted waves produced by the top crystal. They are only visible between point 2 and 8 in Figure 4.

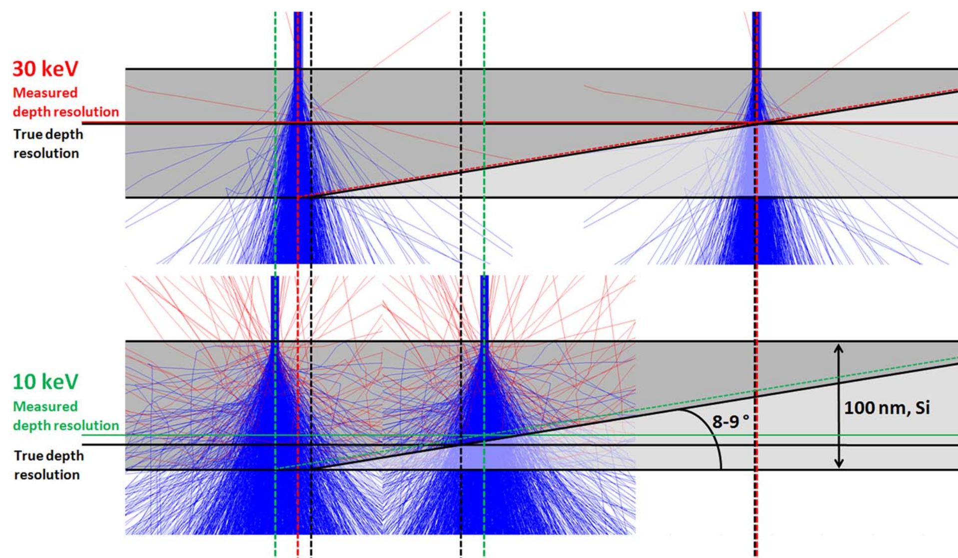

Figure 8. Illustration of the bias introduced by the beam broadening at low incident energy in the evaluation of the depth resolution. The electron trajectories were produced by CASINO (Drouin et al., 2007).

depth resolution by up to 50% at 10 keV, while it should be negligible at 30 keV.

The model above is convenient because it uses the same formalism (i.e., cross sections and mean free paths) as the well spread Monte Carlo simulations of electron trajectories in materials. Alternatively, one can use the formalism that Yamamoto (1977) used to account for the depth resolution of electron channeling patterns, which involves the complex lattice potential for electron diffraction. The complex lattice potential represents inelastic scattering (plasmon, phonon, and single electron excitation altogether) and is introduced to the crystal lattice potential in order to account for the damping of the diffracted wave along its travel. From the mean complex lattice potential V_0^i, a mean absorption coefficient μ_0 can be calculated. For Si, $\mu_0 = V_0^i/54 = 0.012\ \text{nm}^{-1}$ at 100 keV and room temperature (Reimer, 1997: 309). In the nonrelativistic regime, which is a more valid approximation in SEM than in TEM, this mean absorption coefficient μ_0 is inversely proportional to the energy (Hashimoto, 1964), which means that the depth resolution of Kikuchi diffraction in Figure 5 can be expressed approximately by $2.6/\mu_0$. It might be possible to use this simple relationship to rapidly evaluate the depth resolution for any Z and E, because μ_0 is a function of these two parameters (as well as of the temperature, because of the phonon scattering). For example, for Ge, $\mu_0 = 0.026\ \text{nm}^{-1}$ at 100 keV and room temperature (Reimer, 1997: 309). Thus the depth resolution for Ge at 30 keV would be $2.6 \times 30/100/0.026 = 30$ nm and $2.6 \times 10/100/0.026 = 10$ nm at 10 keV. It would be very interesting to validate this relationship between the mean absorption coefficient and the depth resolution of on-axis TKD for other atomic numbers. A first study by Sneddon et al. (2017) with conventional TKD confirms that the depth resolution presents a strong dependence with atomic number. Very interestingly, they report a depth resolution of 80, 33, and 13 nm for Al, Cu, and Pt, respectively. From this result, it

https://doi.org/10.1017/S1431927617012697 Published online by Cambridge University Press

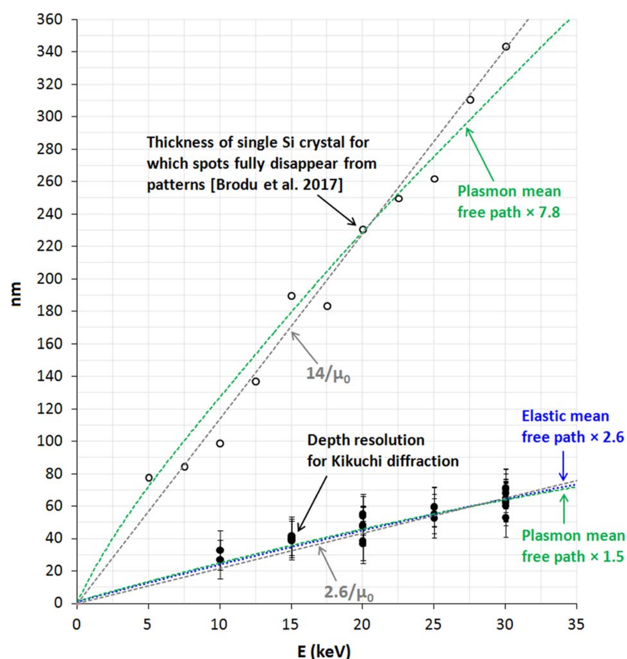

Figure 9. Depth resolution dependence with incident energy by on-axis transmission Kikuchi diffraction in scanning electron microscope for cubic Si. The thickness of single Si crystal for which Bragg diffraction spots disappear completely from patterns is added for comparison (Brodu et al., 2017). The elastic and plasmon mean free paths are taken from Mayol & Salvat (1997) and Shinotsuka et al. (2015), respectively, and the mean absorption coefficient is obtained from Reimer (1997: 309).

might be possible to have a clue on the scattering process responsible for the absorption leading to the depth resolution. The inelastic and elastic mean free path at 30 keV are, respectively, 35, 25, and 19 nm (Shinotsuka et al., 2015) and 24, 7.9, and 3.5 nm (Mayol & Salvat, 1997) for Al, Cu, and Pt. While the depth resolution reported by Sneddon et al. divided by the inelastic mean free path is far from constant with Z (2.3, 1.3, and 0.7), the depth resolution divided by the elastic mean free path is close to constant (3.4, 4.2, and 3.7). It suggest that the electron–nucleus interaction drives the absorption responsible for the depth resolution. Hence, elastic and quasi-elastic (phonon) scattering would be the major contribution, over plasmon scattering, to the depth resolution of TKD.

To go further, it is well known that the damping of a diffracted wave of intensity I along its travel path t, on average (i.e., independently from the crystallographic direction), can be described by the decreasing exponential $I(t) = I_0 \exp(-\mu_0\ t)$ (Ichimiya & Lehmpfuhl, 1978; Spence & Zuo, 1992: 78). Note that the exact same dependence can be obtained by using the previous formalism with the mean free path. Indeed, the probability for a given number of interactions to occur along a travel path of variable length, as given by Poisson's law, is of the same form. This exponential dependence with thickness of the damping observed in Figure 4 could not be confirmed here because profile analysis was unsuccessful (see Methodology for the Determination of the Depth Resolution section). Still, this behavior is highly probable. It is possible to verify that the depth resolution measured and the mean absorption coefficient reported in Reimer (1997: 309) are in line: at 30 keV, a depth resolution of 65 nm was measured (Fig. 5), which gives $I(t)/I_0 = \exp(-\mu_0\ t) = 0.07$, for $t = 65$ nm and $\mu_0\ (E) = 0.012 \times 100/E = 0.041$ at 30 keV (Reimer, 1997: 309). A remaining contrast of 7% is likely to have made the diffraction contrast drop below the threshold for detection, which means that we can make a direct use of the mean absorption coefficient to evaluate the contribution of a layer at a given depth. A first example of the calculation is as follows: in the case of a division of the depth resolution at 30 keV in five layers of 65/5 = 13 nm each, if the bottom layer produces a contrast of 100% (as the most intense contribution on the pattern, it is used as the reference), then the first layer right above it produces a relative contrast of 58%, the next 34%, then 20% and finally the last 12%. If instead the depth resolution reported in Figure 5 is divided into two layers, then the bottom one produces again a contrast of 100% and the one above it produces a relative contrast of 27%. While this calculation was done at 30 keV, these percentages are valid for any incident energy. Alternatively, it is possible to calculate the thickness of the surface layer producing a given percentage of the total diffraction contrast: at 30 keV, a layer of 17 nm produces 50% of the contrast, 34 nm produces 75%, and 56 nm produces 90%.

Finally, we can try to gather Bragg and Kikuchi diffraction inside a common theoretical framework. Like any diffracted wave, Bragg spots are absorbed along their travel inside a crystal. A previous study reported the sample thickness for which Bragg spots in Si disappear from patterns as a function of incident energy (Brodu et al., 2017). At that specific sample thickness (see Fig. 9), the spots were considered absorbed, and the coherence with the incident beam was lost. Unlike Kikuchi diffraction, spots could not "restart" at this point because the coherence with the incident beam is necessary. Kikuchi diffraction on the other hand can still produce diffraction even though the sample is several times thicker than the characteristic length for absorption, because the coherence with the incident beam is not necessary. Unlike spots, Kikuchi diffraction beneficiates from its own in-depth localized sources (Zaefferer, 2007; Winkelmann, 2010). This is the reason why very thick samples still produce Kikuchi diffraction by transmission while spots have long disappeared from patterns, as well as why there is a depth resolution with Kikuchi diffraction, that we can make use of for orientation mapping, while there is none with spots. Another difference lies in the absorption length: it was determined that an average of 7.8 plasmon collisions were necessary for the Bragg diffraction spots to disappear from patterns produced by a single Si crystal (Brodu et al., 2017) (the corresponding number of phonon collisions could not be determined), while it is about 1.5 for Kikuchi diffraction according to the present study. We attribute this difference to the fact that Bragg spots are the direct reflections of the incident beam, while Kikuchi diffraction is not as direct and

https://doi.org/10.1017/S1431927617012697 Published online by Cambridge University Press

requires first the production of a diffuse background by incoherent scattering, from which only a small part produces Kikuchi diffraction according to the small relative intensity in patterns of Kikuchi diffraction in comparison with the background intensity. With overall much less intensity, the Kikuchi diffraction would require much less crystal thickness to drop, by absorption, below the signal/noise ratio of the camera in comparison to spots.

Conclusion

The depth resolution of the on-axis TKD technique in SEM was investigated with a specifically designed and produced twinned cubic silicon bi-crystal. The main conclusions are the following:

- The existence of a depth resolution for TKD can be explained as follows: unlike Bragg diffraction, Kikuchi diffraction beneficiates from emitting sources distributed inside the sample. Hence, each layer of the sample generates independently Kikuchi diffraction. However, the Kikuchi diffraction produced by a layer found at a given depth suffers an absorption on its way out, as a function of the thickness that remains to be crossed. Inevitably this makes the last layers the most visible. Then, because the hardware and software limitations necessarily produce a detection threshold, only the contribution from a finite fraction of these layers, at the bottom, is effectively detected, giving rise to what we call a depth resolution as a finite length, although the absorption responsible for this depth resolution remains essentially a continuous phenomenon. In that sense, a finite depth resolution value is necessarily highly relative and is not an intrinsic property.
- The depth resolution, defined here as the minimal thickness of material at the bottom of the sample such that the material above does not produce a contribution to the Kikuchi diffraction pattern that can be detected to the naked eye, was measured on cubic silicon by on-axis TKD, and ranges from 30 to 65 nm in the range 10–30 keV, with a close to linear dependence with incident energy, while there is no dependence with the total sample thickness. It means that the depth resolution and lateral resolution vary in opposite ways with incident energy.
- The observed linear dependence of the depth resolution with incident energy is the consequence of the mean free paths for phonon, plasmon, and elastic scattering having a linear dependence with energy. In this situation, a fixed number of interactions is responsible for the depth resolution measured. More precisely, the depth resolution measured on silicon corresponds to 1.5 and 2.6 times the plasmon and elastic mean free path, respectively, although it is not currently clear which scattering process in particular, plasmon, phonon, or elastic, is responsible for the absorption at the origin of the depth resolution.
- Alternatively, a simple relationship might provide a rapid evaluation of the depth resolution of on-axis TKD for any incident energy and atomic number from the mean absorption coefficient μ_0. The depth resolution would be given by $2.6/\mu_0$ (E, Z, T). If the dependence of the depth resolution with incident energy can be accounted for by this relationship, the dependence with atomic number remains to be confirmed.
- The absorption producing the depth resolution, making grains less and less visible away from the back surface of the lamella, most likely varies with the exponential of the thickness crossed. In addition to the absorption, a second mechanism was evidenced: the progressive generation of Kikuchi diffraction with increasing grain size. Hence, the contribution of a grain to the Kikuchi pattern depends not only on its position inside the depth resolution layer, but also on its size, meaning that the grains right at the back surface will not always necessarily be the ones contributing most to the Kikuchi pattern. Thus, to better interpret patterns, the generation of Kikuchi diffraction with thickness should also be studied.

Acknowledgments

This work was supported by the French State through the program "Investment in the future" operated by the National Research Agency (ANR) and referenced by ANR-11-LABX-0008-01 (LabEx DAMAS).

References

Bhattacharyya, A. & Eades, J.A. (2009). Use of an energy filter to improve the spatial resolution of electron backscatter diffraction. *Scanning* **31**, 114–121.

Brodu, E., Bouzy, E. & Fundenberger, J.-J. (2017). Diffraction contrast dependence on sample thickness and incident energy in on-axis Transmission Kikuchi Diffraction in SEM. *Ultramicroscopy* **181**, 123–133.

Brodu, E., Bouzy, E., Fundenberger, J.-J., Guyon, J., Guitton, A. & Zhang, Y. (2017). On-axis TKD for orientation mapping of nanocrystalline materials in SEM. *Mater Charact* **130**, 92–96.

Brodusch, N., Demers, H. & Gauvin, R. (2013). Nanometres-resolution Kikuchi patterns from materials science specimens with transmission electron forward scatter diffraction in the scanning electron microscope. *J Microsc* **250**, 1–14.

Crewe, A.V., Wall, J. & Langmore, J. (1970). Visibility of single atoms. *Science* **168**, 1338–1340.

Deal, A., Hooghan, T. & Eades, A. (2008). Energy-filtered electron backscatter diffraction. *Ultramicroscopy* **108**, 116–125.

Dingley, D. (2004). Progressive steps in the development of electron backscatter diffraction and orientation imaging microscopy. *J Micros* **213**, 214–224.

Drouin, D., Couture, A.R., Joly, D., Tastet, X., Aimez, V. & Gauvin, R. (2007). CASINO V2.42 – A fast and easy-to-use modeling tool for scanning electron microscopy and microanalysis users. *Scanning* **29**, 92–101.

Fundenberger, J.J., Bouzy, E., Goran, D., Guyon, J., Yuan, H. & Morawiec, A. (2016). Orientation mapping by transmission-SEM with an on-axis detector. *Ultramicroscopy* **161**, 17–22.

Fundenberger, J.-J., Morawiec, A., Bouzy, E. & Lecomte, J.-S. (2003). Polycrystal orientation maps from TEM. *Ultramicroscopy* **96**, 127–137.

https://doi.org/10.1017/S1431927617012697 Published online by Cambridge University Press

Germer, L.H. (1939). Electron diffraction studies of thin films. I. Structure of very thin films. *Phys Rev* **56**, 58–71.
Hall, C.R. & Hirsch, P.B. (1965). Effect of thermal diffuse scattering on propagation of high energy electrons through crystals. *Proc R Soc A* **286**(1962), 158–177.
Hashimoto, H. (1964). Energy dependence of extinction distance and transmissive power for electron waves in crystals. *J Appl Phys* **35**, 277.
Ichimiya, A. & Lehmpfuhl, G. (1978). Axial channeling in electron diffraction. *Zeitschrift für Naturforschung* **33a**, 269–281.
Keller, R.R. & Geiss, R.H. (2012). Transmission EBSD from 10 nm domains in a scanning electron microscope. *J Microsc* **245**, 245–251.
Mayol, R. & Salvat, F. (1997). Total and transport cross sections for elastic scattering of electrons by atoms. *Atomic Data Nuclear Data Tables* **65**, 55–154.
Morawiec, A., Bouzy, E., Paul, H. & Fundenberger, J.-J. (2014). Orientation precision of TEM-based orientation mapping techniques. *Ultramicroscopy* **136**, 107–118.
Ren, S.X., Kenik, E.A., Alexander, K.B. & Goyal, A. (1998). Exploring spatial resolution in electron back-scattered diffraction experiments via Monte Carlo simulation. *Microsc Microanal* **4**, 15–22.
Reimer, L. (1997). *Transmission Electron Microscopy: Physics of Image Formation and Microanalysis*, Vol. 36 (4th ed.). Berlin: Springer Series in Optical Sciences.
Rice, K.P., Keller, R.R. & Stoykovich, M.P. (2014). Specimen-thickness effects on transmission Kikuchi patterns in the scanning electron microscope. *J Microsc* **254**, 129–136.
Shinotsuka, H., Tanuma, S., Powell, C.J. & Penn, D.R. (2015). Calculations of electron inelastic mean free paths. X. Data for 41 elemental solids over the 50eV to 200keV range with the relativistic full Penn algorithm. *Surf Interf Anal* **47**, 871–888.
Sneddon, G.C., Trimby, P.W. & Cairney, J.M. (2016). Transmission Kikuchi diffraction in a scanning electron microscope: A review. *Mater Sci Eng R* **110**, 1–12.
Sneddon, G., Trimby, P. & Cairney, J. (2017). The influence of microscope and specimen parameters on the spatial resolution of transmission Kikuchi diffraction. *Microsc Microanal* **23**(Suppl 1), 532–533.
Spence, J.C.H. & Zuo, J.M. (1992). *Electron Microdiffraction*. New York: Springer Science + Business Media New York.
Suzuki, S. (2013). Features of transmission EBSD and its application. *JOM* **65**, 1254–1263.
Tanuma, S., Powell, C.J. & Penn, D.R. (2011). Calculations of electron inelastic mean free paths. IX. Data for 41 elemental solids over the 50 eV to 30 keV range. *Surf Interf Anal* **43**, 689–713.
Tee, I., Li, K., Liu, P., Du, A., Seah, S. & Fidelia, T. (2009). Study of low-kv cleaning method to improve TEM samples prepared by FIB. In *IEEE Proceedings of 16th IPFA*, pp. 552–554. Nanjing, China: IEEE.
Trimby, W. (2012). Orientation mapping of nanostructured materials using transmission Kikuchi diffraction in the scanning electron microscope. *Ultramicroscopy* **12**, 16–24.
Trimby, P.W., Cao, Y., Chen, Z., Han, S., Hemker, K.J., Lian, J., Liao, X., Rottmann, P., Samudrala, S., Sun, J., Wang, J.T., Wheeler, J. & Cairney, J.M. (2014). Characterizing deformed ultrafine-grained and nanocrystalline materials using transmission Kikuchi diffraction in a scanning electron microscope. *Acta Mater* **62**, 69–80.
van Bremen, R., Ribas Gomes, D., de Jeer, L.T.H., Ocelík, V. & De Hosson, J.T.M. (2016). On the optimum resolution of transmission-electron backscattered diffraction (t-EBSD). *Ultramicroscopy* **160**, 256–264.
Vespucci, S., Winkelmann, A., Mingard, K., Maneuski, D., O'Shea, V. & Trager-Cowan, C. (2017). Exploring transmission Kikuchi diffraction using a Timepix detector. *J Instrum* **12**, 1–8.
Vespucci, S., Winkelmann, A., Naresh-Kumar, G., Mingard, K.P., Maneuski, D., Edwards, P.R., Day, A.P., O'Shea, V. & Trager-Cowan, C. (2015). Digital direct electron imaging of energy-filtered electron backscatter diffraction patterns. *Phys Rev B* **92**, 205301.
Wang, Y.Z., Kong, M.G., Liu, Z.W., Lin, C.C. & Zeng, Y. (2016). Effect of microscope parameter and specimen thickness of spatial resolution of transmission electron backscatter diffraction. *J Microsc* **264**, 34–40.
Wilkinson, A.J., Moldovan, G., Britton, T.B., Bewick, A., Clough, R. & Kirkland, A.I. (2013). Direct detection of electron backscatter diffraction pattern. *Phys Rev Lett* **111**, 065506.
Williams, D.B. & Barry Carter, C. (1996). *Transmission Electron Microscopy – A Text Book for Material Science*. New York: Springer Science.
Winkelmann, A. (2010). Principles of depth-resolved Kikuchi pattern simulation for electron backscatter diffraction. *J Microsc* **239**, 32–45.
Wisniewski, W., Saager, S., Böbenroth, A. & Rüssel, C. (2017). Experimental evidence concerning the significant information depth of electron backscatter diffraction (EBSD). *Ultramicroscopy* **173**, 1–9.
Yamamoto, T. (1977). Experimental aspects of electron channeling patterns in scanning electron microscopy II. Estimation of contrast depth. *Phys Status Solidi A* **44**, 467.
Yuan, H., Brodu, E., Chen, C., Bouzy, E., Fundenberger, J.-J. & Toth, L.S. (2017). On-axis versus off-axis transmission Kikuchi diffraction technique: Application to the characterization of severe plastic deformation induced ultrafine grained microstructures. *J Microsc* **267**, 70–80.
Zaefferer, S. (2007). On the formation mechanisms, spatial resolution and intensity of backscatter Kikuchi patterns. *Ultramicroscopy* **107**, 245–266.

https://doi.org/10.1017/S1431927617012697 Published online by Cambridge University Press